

THE MAJOR CAUSE OF BRIDGE COLLAPSES ACROSS ROCK RIVERBEDS: SHEAR BANDING

Tse-Shan Hsu

Professor, Department of Civil Engineering, Feng-Chia University
President, Institute of Mitigation for Earthquake Shear Banding Disasters
Taiwan, R.O.C.
tshsu@fcu.edu.tw

Po Yen Chuang

Ph.D Program in Civil and Hydraulic Engineering
Feng-Chia University, Taiwan, R.O.C.

Kuan-Tang Shen

Secretary-General, Institute of Mitigation for Earthquake Shear Banding Disasters
Taiwan, R.O.C.

Fu-Kuo Huang

Associate Professor, Department of Water Resources and Environmental Engineering
Tamkang University, Taiwan, R.O.C.

Abstract

Current performance design codes require that bridges be designed that they will not collapse within their design life. However, in the past twenty five years, a large number of bridges have collapsed in Taiwan, with their actual service life far shorter than their design life. This study explores the major cause of the collapse of many these bridges. The results of the study reveal the following. (1) Because riverbeds can be divided into high shear strength rock riverbeds and low shear strength soil riverbeds, the main cause of bridge collapse on a high shear strength rock riverbed is the shear band effect inducing local brittle fracture of the rock, and the main cause on a low shear strength soil riverbed is scouring, but current bridge design specifications only fortify against the scouring of low shear strength soil riverbeds. (2) Since Taiwan is mountainous, most of the collapsed bridges cross high shear strength rock riverbeds in mountainous areas and, therefore, the major cause of collapse of bridges in Taiwan is that their design does not consider the

shear band effect. (3) Because shear banding will induce local deep grooving of the high shear strength rock riverbed, foundations embedded in the shear band will induce the softening of the overall bridge stiffness during continuous exposure, and subsequently collapse after complete exposure. Therefore, it is suggested that the bridge design code must account for the shear band effect to ensure the stability of bridges crossing low shear strength rock riverbeds.

Keywords: bridges, collapse, scouring, soil riverbed, shear banding, rock riverbed.

Introduction

Taiwan is located on the edge of the Eurasian continental plate. Many mountains formed in Taiwan under the lateral compression of the Philippine Sea Plate; and due to the needs of people's lives, economic development, and

tourism development, many roads and bridges were built in mountain areas. Therefore, a relatively large number of bridges crossed high shear strength riverbeds (Figure 1), while a few bridges cross low shear strength soil riverbeds (Figure 2).



Figure 1. A bridge across a high shear strength rock riverbed with shear bandings.



Figure 2. A bridge across a low shear strength soil riverbed.

It has been found that over a hundred bridges have collapsed in Taiwan in the past 25 years. Moreover, the actual service life of the collapsed bridges similar to those shown in Fig-

ures 3 and 4 is only 9 to 35 years. This is far shorter than the design life of 100 to 120 years prescribed by the specifications of various countries.



Figure 3. The collapse of Pifeng Bridge in Taichung, Taiwan, during the 1999 Jiji earthquake.



Figure 4. The collapse of Houfeng Bridge in Taichung, Taiwan, during Typhoon Sinlaku in 2008 (Jeng, 2008).

The largest number of bridge collapses in Taiwan occurred during Typhoon Morakot in 2009. Most previous scholars have attributed the bridge collapse to riverbed scouring (Chiu *et al.*, 2012).

For Houfeng Bridge, shown in Figure 4 after its collapse during Typhoon Sinlaku, if riverbed scouring was the primary cause of its collapse, the peak flow of $4,563 \text{ m}^3/\text{s}$ of the Dajiayi Basin passing through Shi-

gangba station during the typhoon's transit should be the largest. However, Table 1 shows that the maximum peak flow was instead $5,873 \text{ m}^3/\text{s}$ during the passage of Typhoon Mindulle. Based on the fact that the riverbed scouring failed to meet the three required conditions of disaster causes, Hsu and Hsieh (2009) found that riverbed scouring was not the major cause for the collapse of Houfeng Bridge.

Table 1. The peak flow of the Dajiayi Basin passing through Shigangba station during 2004-2008 (Hsu and Hsieh, 2009).

	Date	Peal flow (m ³ /sec)
Typhoon Mindulle	2004.07.03	5,873
Typhoon Aere	2004.08.25	3,912
Typhoon Haitang	2004.07.19	2,926
Typhoon Matsa	2005.08.05	3,535
Typhoon Talim	2005.09.01	1,217
Typhoon Longwang	2005.10.02	1,855
Typhoon Bilis	2006.07.14	1,665
Typhoon Sepat	2007.08.13	2,423
Typhoon Wipha	2007.08.19	2,087
Typhoon Krosa	2007.10.06	2,873
Typhoon Kalmaegi	2008.07.18	2,890
Typhoon Fung-wong	2008.07.28	2,131
Typhoon Sinlaku	2008.09.14	4,563

As bridge collapses can cause injuries and traffic disruptions, bridge disaster mitigation is the responsibility of bridge authorities around the world. In Taiwan, bridge disaster mitigation has been a long-term problem with bridge authorities failing to produce countermeasures to prevent collapses. In this paper, a collapse mechanism for

a bridge across high shear strength rock riverbed is first proposed. Then, a numerical simulation of the weakening of Houfeng Bridge induced by deep grooving is performed. Finally, taking the Zhongzheng Bridge as an example, the influence of the shear band effect on bridge collapse is studied, and an improvement method is proposed.



Note: In the figure above, a is the toppled caisson, and b is the fallen bridge deck.

Figure 5. The collapse of Houfeng Bridge during Typhoon Sinlaku.

Previous studies in the field of hydraulic engineering have argued that the cause of bridge failure was riverbed scouring (Department of Transport and Main Roads, State of Queensland, 2013; Keaton *et al.*, 2012; Khan, 2015; Lagasse *et al.*, 2001; Warren, 2011). While Figure 6 shows heavy scouring does occur in low shear strength soil riverbeds, for a high shear strength rock riverbed, this riverbed scouring mechanism is obviously not applicable. Therefore, this study proposes a new

collapse mechanism for a bridge across a high shear strength rock riverbed.

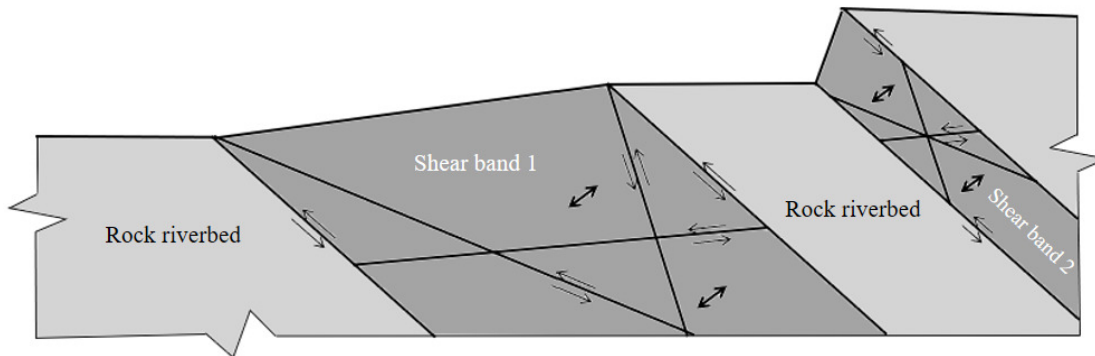
Proposed Collapse Mechanism for Bridges Crossing High Shear Strength Rock Riverbeds

Figure 4 shows the Houfeng Bridge collapse during Typhoon Sinlaku. Figure 5 shows the in-situ conditions of the exposed caissons, the toppled caissons, and the fallen bridge decks after Typhoon Sinlaku.



Figure 6. A bridge on a low shear strength soil riverbed that remained stable after group pile foundations were severely exposed (Sijhou Bridge, Changhua, Taiwan).

- 1) Generally, high shear strength rock riverbeds are formed during tectonic earthquakes, resulting in localized shear bands (see Figure 7).



Note: Shear band 1 is highly brittle fractured; and shear band 2 is slightly brittle fractured.

Figure 7. A high shear strength rock riverbed with localized shear bands.

2) At present, seismic bridge design codes only require the fortification of the secondary effect (*i.e.*, ground vibrations) of tectonic earthquakes. When the main effect (*i.e.*, the shear

band effect) is completely neglected in the design, the bridge abutments and a part of the caisson foundations will be embedded in the shear bands (see Figure 8).

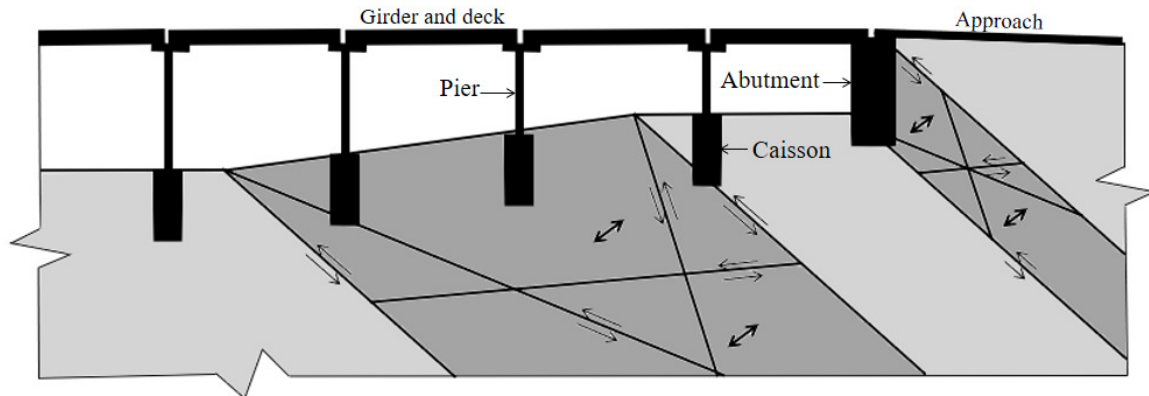


Figure 8. Bridge with abutments and caissons embedded in a rock riverbed.

3) Figure 9 shows that the degree of brittle fracture of the rock riverbed in the shear band will continue to increase during tectonic earthquakes. The highly brittle-fractured shear-

band rocks will be lost in a flood, which will cause deep grooves to form in the riverbed. Furthermore, both sides of the deep groove are shear-banding tilted slopes.



Note: In the figure above, a denotes a deep groove, b denotes a shear-band tilted slope, and c denotes a non-shear-band rock riverbed.

Figure 9. The rock riverbed in the Dajiaxi Basin, in Taichung, Taiwan.

4) After the formation of the deep groove in the rock riverbed, its depth will increase as a result of the continuous loss of brittle-fractured shear-band rocks during flooding.

When all the shear-band rocks around a caisson or group piles are lost (see Figure 10), the bridge will collapse (Figures 4 and 5).

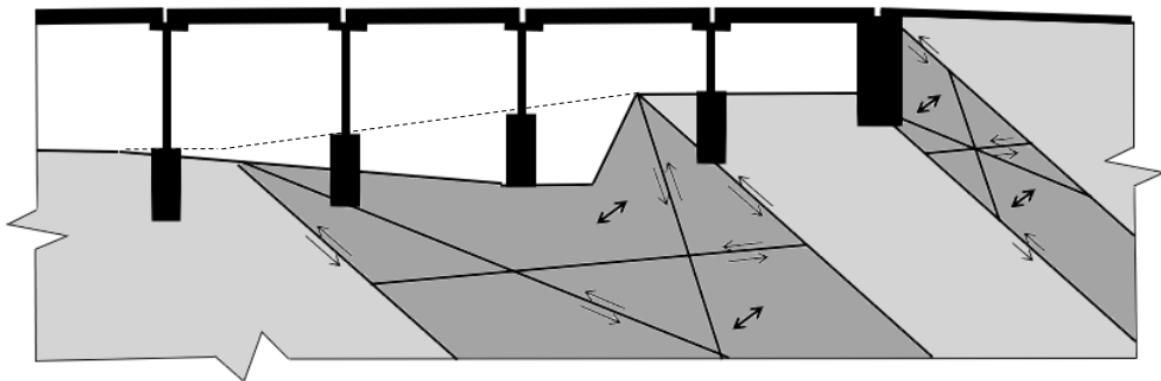


Figure 10. The loss of brittle-fractured shear-band rocks around caissons.

Case Study

Problem description

The Zhongzheng Bridge in Hsinchu, Taiwan, was completed in

1981. Since the degree of brittle-fractured shear-band rocks continued to increase after construction, a concrete-groundsill was added in 2003 (see Figure 11).



Figure 11. The construction of a concrete-groundsill downstream of the Zhongzheng Bridge completed in 2003 (Google Earth, 2020).

The high shear strength concrete-groundsill started to fracture in 2007, and while the degree of brittle fracture gradually increased from the left bank to the right bank of the deep groove downstream of the bridge, the situation was not serious (see Figure 12). During Typhoon Saola in August 2012, the deep grooving effect of the shear-band rock riverbed intensified. The caissons

embedded in the shear bands were severely exposed, and the concrete-groundsill in the deep groove failed and was lost. In addition to extending towards the left bank downstream of the Zhongzheng Bridge, the range of loss also extended toward the upstream shear-band rock riverbed (see Figure 12(b)).



(a) In 2007 (Bicyclist, 2007)



(b) After Typhoon Saola in August 2012 (Lian, 2013)

Figure 12. The degree of brittle fracture of the concrete-groundsill within the shear-band rock riverbed continued to increase before the collapse of the Zhongzheng Bridge.

After Typhoon Saola in 2012, the reconstruction of a concrete-groundsill on the left bank of the deep groove was completed quickly, as shown in Figure 13. However, during Typhoon Soulik in 2013, a caisson was completely exposed, so the Zhongzheng Bridge collapsed. The pier, cap beam, and bridge decks on both sides of the caisson fell

onto the riverbed. Figure 13 further shows that, after the collapse of the Zhongzheng Bridge, the concrete-groundsill on the left bank of the deep groove of the rock riverbed was slightly damaged, while the deep groove of the rock riverbed extended to the riverbed outside the concrete-groundsill.



Figure 13. Satellite image of the partial drop of the Zhongzheng Bridge in 2013 (Google Earth, 2020).

The reconstruction of the Zhongzheng Bridge was completed in 2015, with the type of the bridge changed from a PCI-girder bridge to a cable-stayed bridge with a total length of 855.3 m, a width of 30 m, a main

tower height of 83.5 m, and a foundation depth of 28 m, as shown in Figure 14. The main purpose of this change was to reduce the contraction scour via a substantial reduction in the number of piers.



(a) Satellite imagery



(b) *In-situ* imagery

Figure 14. The Zhongzheng Bridge after reconstruction in 2015 (Google Earth, 2020).

For a cable-stayed bridge, all steel cable tension is transmitted to the foundation through the main tower, and then to the rock riverbed through the foundation. The rock riverbed therefore needs a high shear strength and low compressibility in order to provide the main tower foundation with the bearing capacity needed for stable cable-stayed bridges.

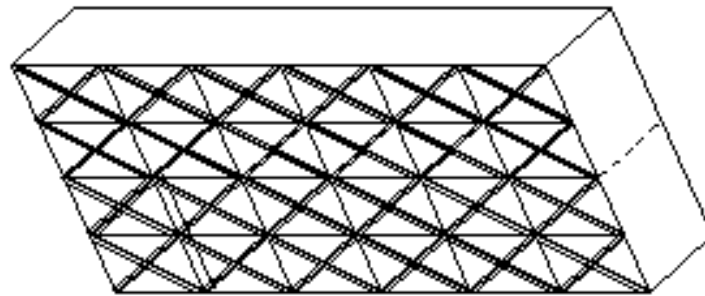
When the rock riverbed adjacent to the main tower foundation does not contain shear bands, the rock riverbed has a high strength and low compressibility, so it can provide the main tower foundation with the bearing capacity and compressibility required to stabilize the cable-stayed bridge within its design life. If the foundation of the main tower is embedded in the shear

band, then the degree of brittle fracture of the shear-band rock riverbed will continue to increase during tectonic earthquakes, which will cause a significant decrease in strength and a significant increase in compressibility. If the bearing capacity is insufficient or the compressibility is too large for the shear-band rock riverbed, the Zhongzheng Bridge will collapse again.

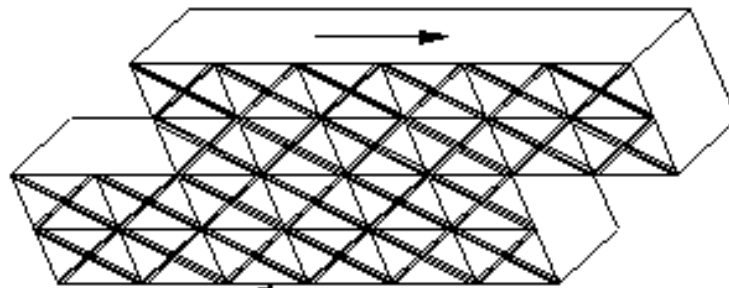
Identification of Shear Bands or Shear Texture

Definition of shear bands

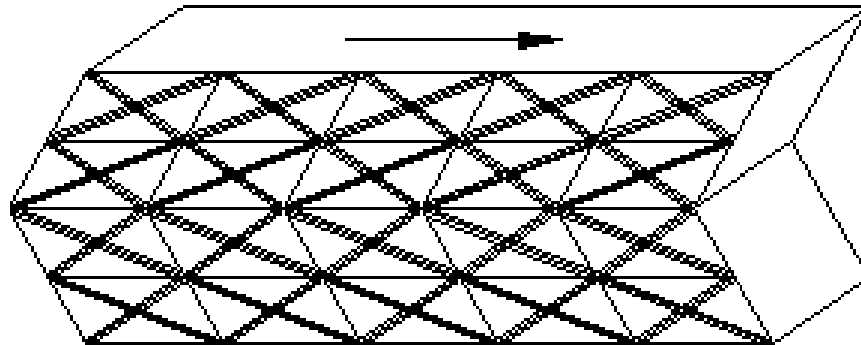
Hertzberg (1983) defined slip and twinning types of shear bands (see Figure 15).



(a) Block before a shear



(b) Slip-type shear-band block

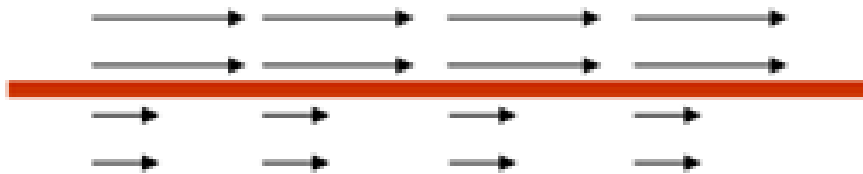


(c) Twinning-type shear-band block

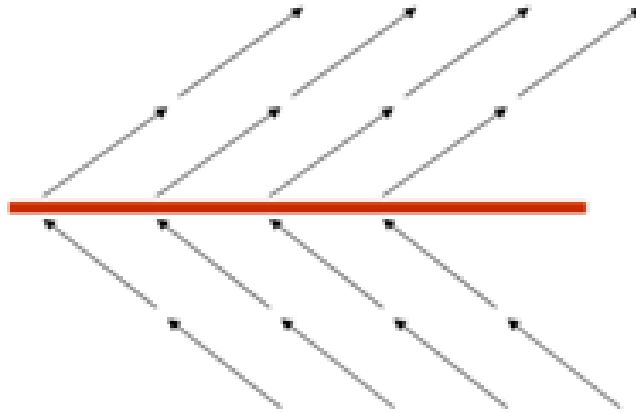
Figure 15. Two types of shear bands as defined by Hertzberg (1983).

The two different types of shear bands shown in Figure 15 can also be defined via a velocity-vector distribution diagram (Hsu, 1987). When the velocity vectors of two adjacent points have the same direction yet different magnitudes, the shear band between

the two points is defined as a slip type (see Figure 16(a)). Conversely, when the velocity vectors have different directions and the same magnitude, the shear band between the two points is defined as a twinning type (see Figure 16(b)).



(a) Slip-type shear band (red line)



(b) Twinning-type shear band (red line)

Figure 16. Definitions of the two different types of shear bands via a velocity-vector distribution map (Hsu, 1987).

Definition of shear textures in the overall shear band width

For the overall shear band width (see Figure 17) between a pair of prin-

cipal deformation shears, Tchalenko (1968) defined shear textures such as thrust shear, Riedel shear, conjugate Riedel shear, and compression texture.

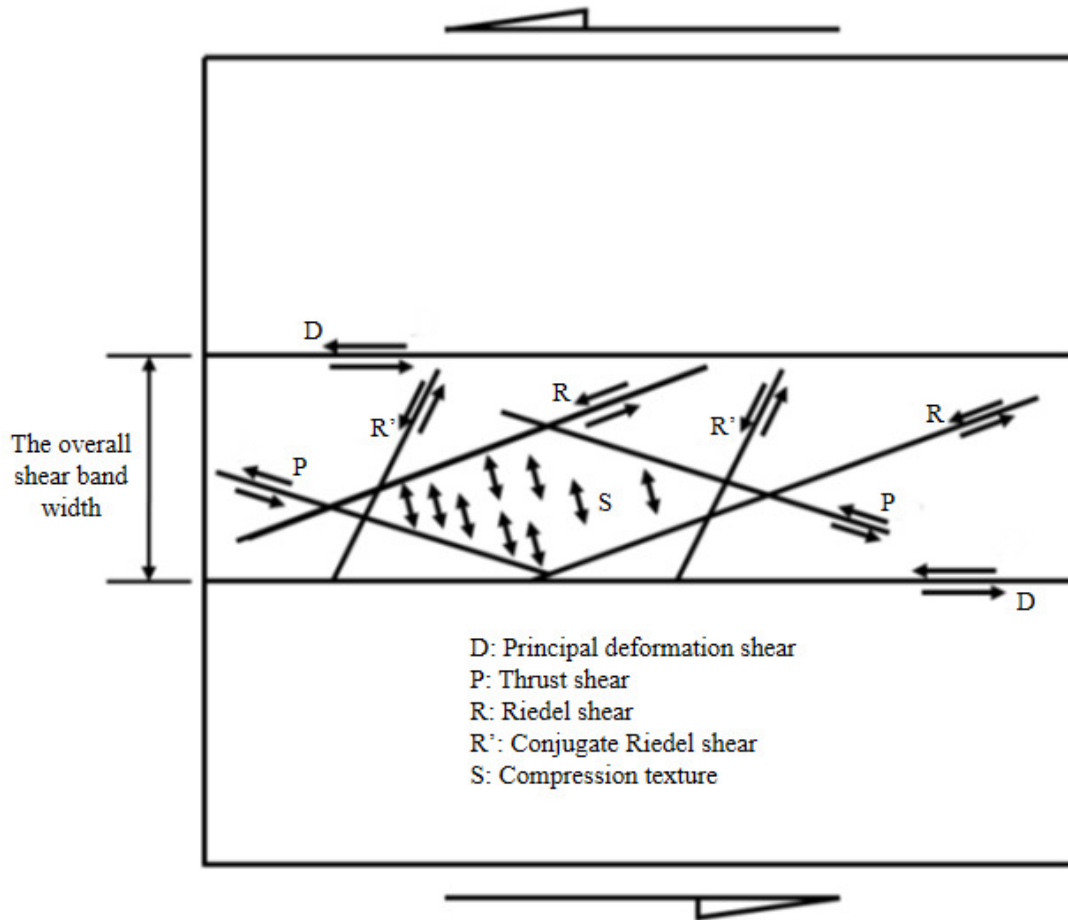


Figure 17. Various shear textures defined in the overall shear band width (Tchalenko, 1968).

Identification of in-situ shear bands or in-situ shear texture

1) Identification of shear bands using the epicenter distribution map
The rock riverbed of the Zhongzheng Bridge is taken as an example. Figure 18 shows the epicenter

distribution map from 1995 to 2017. From this epicenter distribution map, three shear bands passing through the rock riverbed in the Zhongzheng Bridge can be identified, and their strikes are N65°W (white line), N25°E (yellow line), and N65°E (red line).

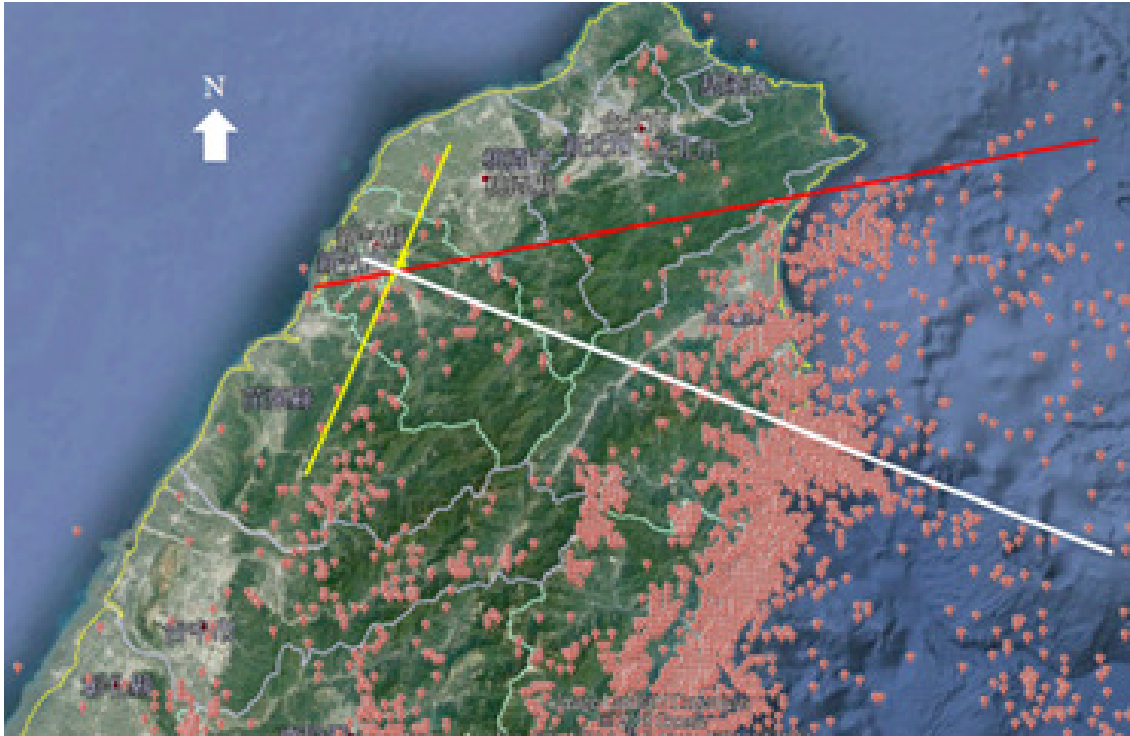


Figure 18. Shear bands with different strikes through the rock riverbed of the Zhongzheng Bridge as identified by the distribution of epicenters (background map from Google Earth, 2020, and epicenter data from the Central Weather Bureau, 2020)

2) Identification of shear bands by displacement landform features

Figure 19 shows a satellite image that includes the rock riverbed of the Zhongzheng Bridge. Three shear bands

passing through it can be identified from displacement landform features, and their strikes are N65°W (white line), N25°E (yellow line), and N65°E (red line).

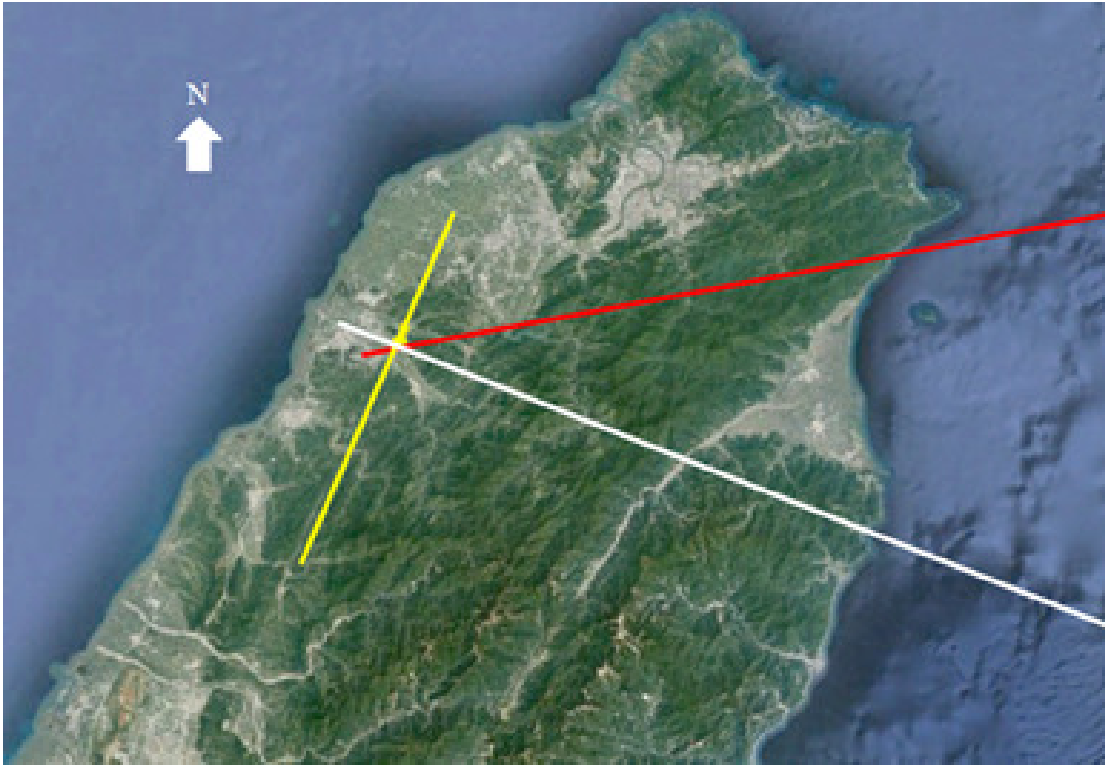


Figure 19. Shear bands identified by displacement landform features (background image from Google Earth, 2020).

3) Identifying shear bands using a GPS velocity-vector distribution map

Figure 20 shows the GPS velocity-vector distribution map from January 1, to December 31, 2007. From this

GPS velocity-vector distribution map, two shear bands across the rock riverbed at the Zhongzheng Bridge can be identified, and their strikes are $N65^{\circ}W$ (white line) and $N25^{\circ}E$ (yellow line).



Figure 20. Shear bands identified from the GPS velocity-vector distribution map (background image from Google Earth, 2020, and GPS velocity vectors from GPS LAB, 2007).

4) Identification of shear textures in the overall shear band width
Enlarging the satellite image shows the displacement landform features of the area adjacent to the Zhongzheng Bridge (see Figure 21). A pair of principal deformation shears (white lines) with a N65°W strike is regarded as the shear band, and within

the overall shear band width, a thrust shear with a N25°W strike (yellow dotted line), a Riedel shear with a N80°W strike (green line), a conjugated Riedel shear with a N65°E strike (yellow line), and a compression texture with a N25°E strike (double arrow line) are identified.

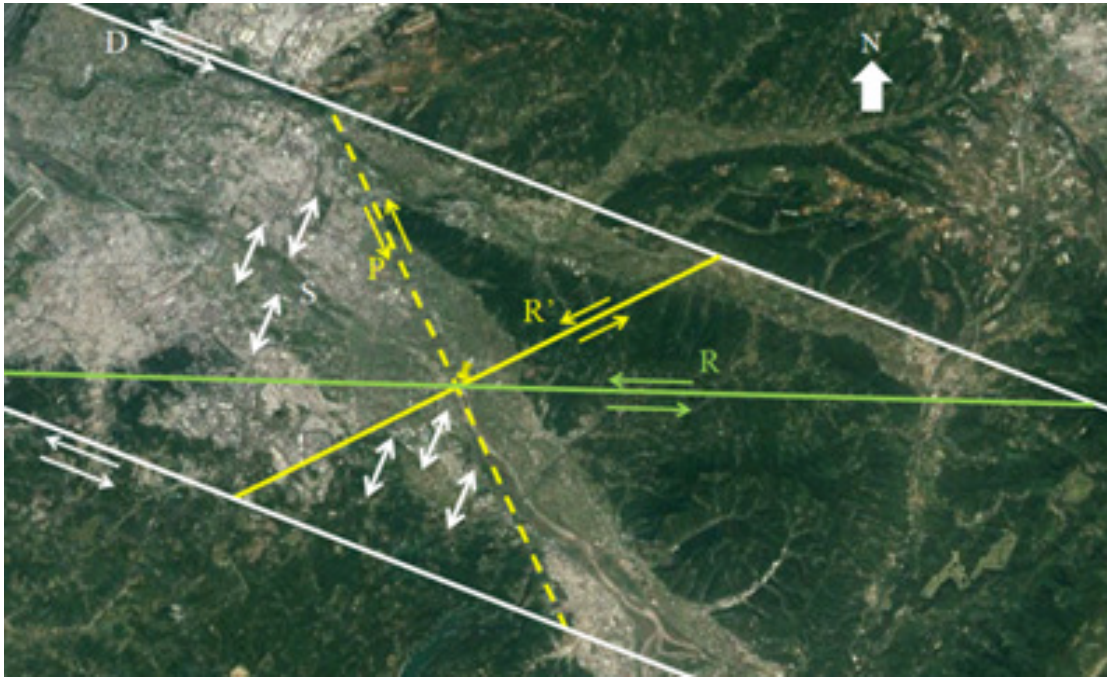


Figure 21. Various shear textures identified within the overall shear band width (background image from Google Earth, 2020).

5) Discussion

Based on the above-mentioned identification results, it is known that there are six different shear bands (or shear textures) in the rock riverbed for the Zhongzheng Bridge (see Figure 22). As shown in Figure 23(a), owing to the continuous displacement of these six shear bands (or shear textures), the brittle-fractured rocks surrounding the C1 and C2 caissons were partially lost during the 2012 Typhoon Saola, causing the C1 and C2 caissons to be exposed, with the C1 caisson more exposed than the C2 caisson. Furthermore, as shown in Figure 23(b), a stepped deep grooving appears in the shear-

band rock riverbed when the bridge collapses. The first-stage deep groove's surface dropped to a depth of 2.5m below the top of the caisson, and the second-stage deep groove's surface dropped below the bottom surface of the C1 caisson, with the C1 caisson toppling because it lost all its bearing capacity. Secondly, a ring-shaped empty space of approximately 70cm in width (see Figure 23(c)) appeared in the C2 caisson, owing to the loss of brittle-fractured shear-band rocks. This phenomenon shows that, once the caisson is embedded in the shear band, the surrounding brittle-fractured shear-band rocks are easily lost.



Figure 22. Shear bands that induced the collapse of the Zhongzheng Bridge (background image from Google Earth, 2020).



(a) During Typhoon Saola in August 2012



(c) Stepped deep grooving of shear-band rock riverbed
after Typhoon Soulik in 2013



(d) The annular empty space that appeared after the loss of shear-band rocks that bounded the C2 caisson in Figure 23(b)

Figure 23. Caissons exposed as a result of deep grooving of the rock riverbed and the loss of brittle-fractured shear-band rocks.

Numerical Analysis of the Houfeng Bridge

Structural analysis model

The Houfeng Bridge comprises structural elements including bridge decks, prestressed I-beams, cap beams, piers, caissons, and the neighboring very stiff soils. Figure 24 shows the

structural model for finite element analysis built in the SAP2000 software, where the x -axis denotes the direction of the bridge axis, the y -axis is the direction of water flow, and the z -axis is the vertical direction. The origin of the Cartesian coordinate system is located on the northern bank of the bridge at the downstream side.

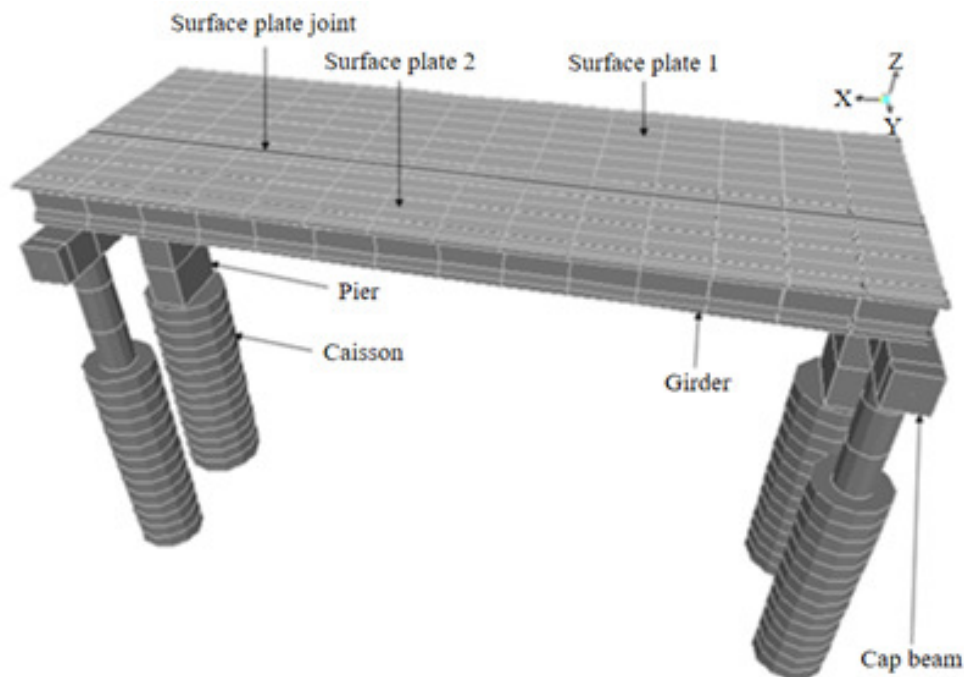


Figure 24. Structural model of the Houfeng Bridge.

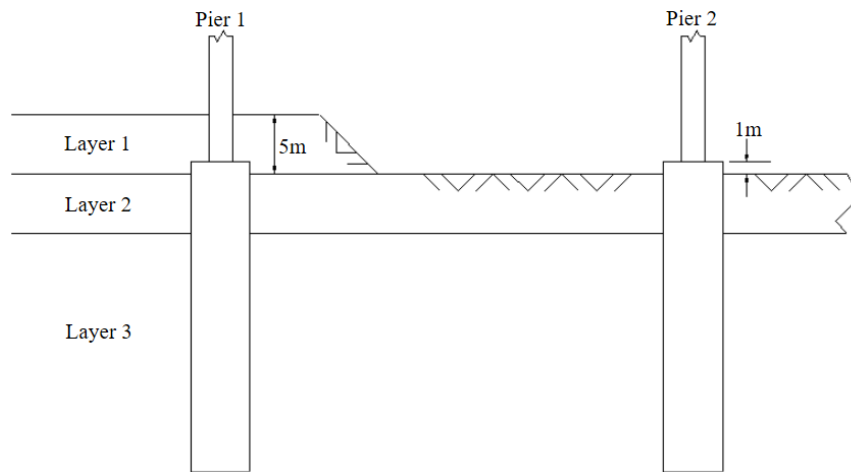
Geometric conditions

As structural elements, where L denotes length, H denotes height, T denotes thickness, W denotes width, and D denotes diameter, the surface reinforced concrete (RC) plates have dimensions of $L = 93$ m, $W = 22$ m, and $T = 25$ cm.

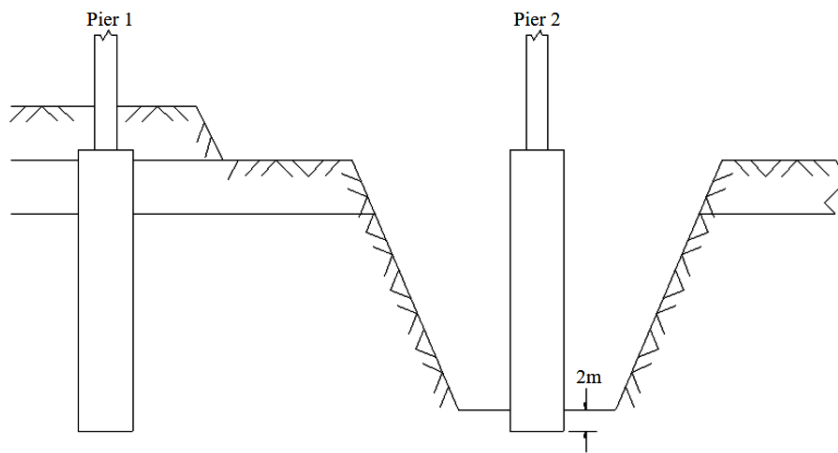
The prestressed I-girders have a length of $L = 93$ m, with an upper web of $W = 0.5$ m, a lower web with $W = 0.5$ m, and $H = 2.8$ m. For the cap beams, $L = 11.8$ m, $W = 2.1$ m, and $H = 3$ m. For the piers, $D = 2.6$ m and $H = 11$ m, while for the caissons $D = 2.6$ m and $H = 11$ m. Very stiff soil layers confining the piers or caissons are categorized into two types, as shown in

Figure 25, based on different analysis conditions. In Case 1, except for the riverbank, the riverbed has a grooving of 1m under the top of the caisson

foundations. In Case 2, some portions of the riverbed have deep grooving effect down to 2m above the bottom of the caisson foundations.



(a) Case 1: without the shear band effect



(b) Case 2: with the shear band effect

Figure 25. Distribution of very stiff soil layers adjacent to piers and caissons, with partial deep grooving effect of the riverbed.

Boundary conditions

The Houfeng Bridge comprises four sub-bridges arranged in parallel, each with respective caissons, piers, cap beams, girders, and decks. Sub-bridge girders are arranged in a layout of 3-4-4-3 in respective sub-bridges, and between every two expansion joints lies the bridge deck slab of each sub-bridge, which is a combined slab formed by two sub-slabs each on the left and on the right.

From the design of the slab, it appears that the joint between the two sub-slabs is in the form of a constraint equation for the three directional displacements U_x , U_y , and U_z . From the design of the girders and cap beams, it appears that the joint between the girder and the cap beam forms a constraint in the two directional displacements U_y and U_z . While connections between very stiff soils and piers or caissons are simulated by spring elements, since the caisson bottoms are seated onto rock layers, the bottom is in the form of a restraint to the three directional displacements U_x , U_y and U_z .

Material properties

For the girder, its concrete strength is $f'_c = 350 \text{ kgf/cm}^2$, its density is 2.345 t/m^3 , Poisson's ratio is 0.2, the Young's modulus is $351,781 \text{ kgf/cm}^2$, the damping ratio is 5%, the cross-sectional area of the steel strand is 62.34 mm^2 , the ultimate strength is $f'_s = 16,500 \text{ kgf/cm}^2$, the yield

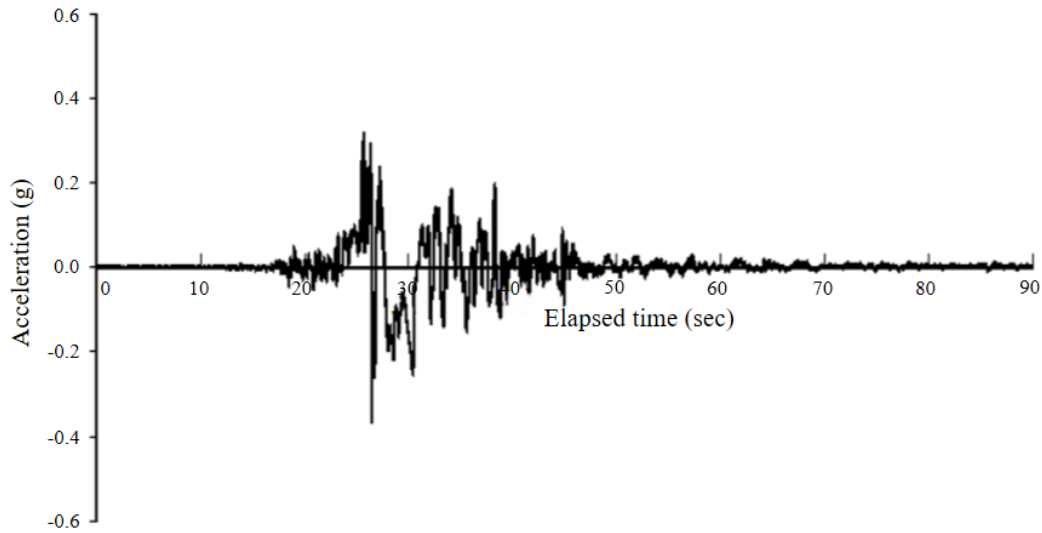
strength is $f_{py} = 13,500 \text{ kgf/cm}^2$, the coefficient of elasticity is $E_{sp} = 1.97 \times 10^6 \text{ kgf/cm}^2$, the curve friction coefficient is $\mu = 0.25/\text{rad}$, the wave influence coefficient is $\kappa = 4.9 \times 10^{-3} \text{ m}^{-1}$, and the slip of the prestressed tendon is $\Delta_1 = 0.8 \text{ cm}$. For the slab and cap beam concrete, the strength is $f'_c = 210 \text{ kgf/cm}^2$, the density is 2.345 t/m^3 , Poisson's ratio is 0.2, and the Young's modulus is $301,869 \text{ kgf/cm}^2$. The pier and caisson concrete has a strength of $f'_c = 280 \text{ kgf/cm}^2$, a density of 2.345 t/m^3 , a Poisson's ratio of 0.2, and a Young's modulus of $327,777 \text{ kgf/cm}^2$.

For the deformed steel bars, $f_y \cong 2800 \text{ kgf/cm}^2$ when the diameter of the steel bars is less than 16 mm and $f_y \cong 4200 \text{ kgf/cm}^2$ when the diameter is greater than 19 mm.

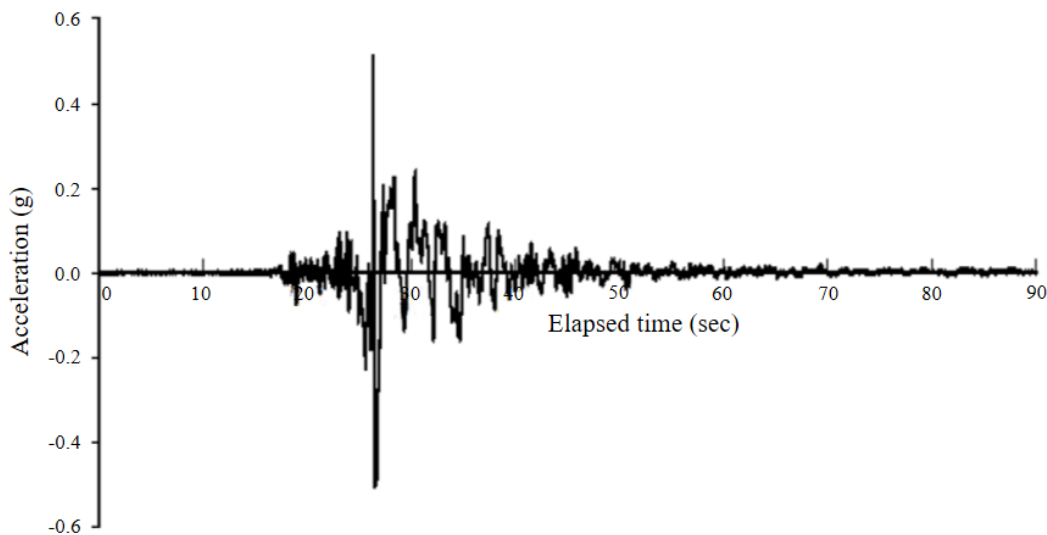
For the very stiff soil springs in Case 1 for the old bridge, the horizontal coefficient of elasticity of Layer 1 soil is $135,147 \text{ kgf/cm}$ and the vertical coefficient of elasticity is $793,454 \text{ kgf/cm}$. The horizontal coefficient of elasticity of Layer 2 soil is $290,388 \text{ kgf/cm}$ and the vertical coefficient of elasticity is $1,586,908 \text{ kgf/cm}$. The horizontal coefficient of elasticity of Layer 3 soil is $454,241 \text{ kgf/cm}$ and the vertical coefficient of elasticity is $2,380,362 \text{ kgf/cm}$. For the very stiff soil springs in Case 2 for the old bridge, except for Pier 2, the horizontal coefficient of elasticity of Layer 1 soil is $49,170 \text{ kgf/cm}$ and the vertical coefficient of elasticity is $317,382 \text{ kgf/cm}$. The horizontal coefficient of elasticity of Layer 2 soil is $105,651 \text{ kgf/cm}$ and

the vertical coefficient of elasticity is 634,763 kgf/cm. The horizontal coefficient of elasticity of Layer 3 soil is 165,265 kgf/cm and the vertical coefficient of elasticity is 952,145 kgf/cm.

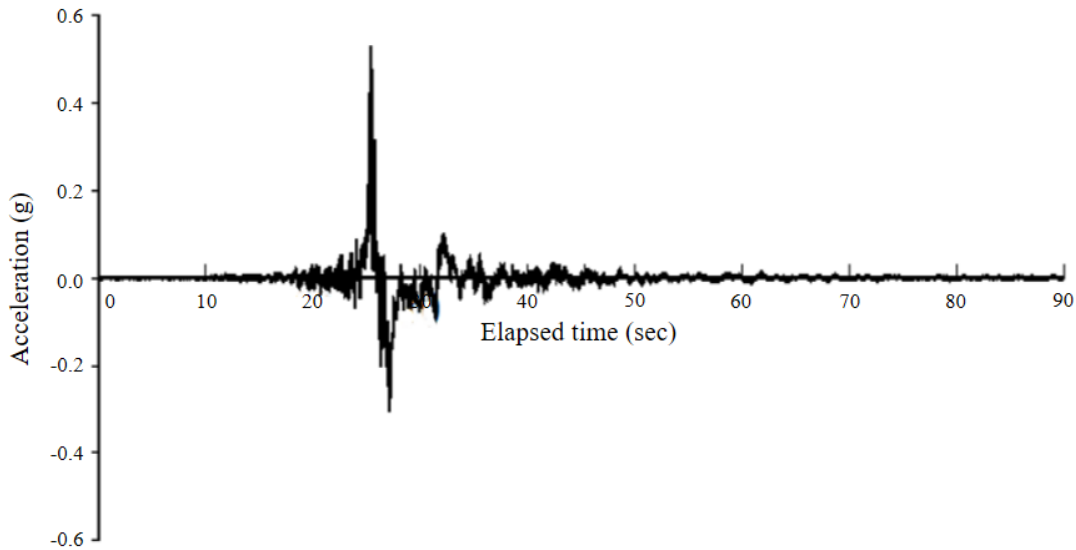
For Pier 2, the horizontal coefficient of elasticity of Layer 3 soil is 62,898 kgf/cm and the vertical coefficient of elasticity is 396,727 kgf/cm.



(a) North-south component



(b) East-west component



(c) Vertical component

Figure 26. Accelerogram of the 1999 Jiji Earthquake, recorded at Shigang Primary School, Taiwan (data from the Central Weather Bureau, 2020).

Modal analysis results

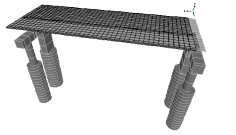
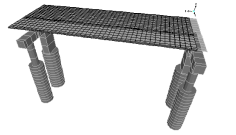
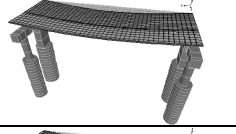
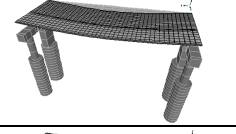
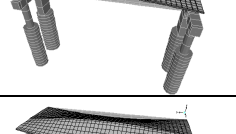
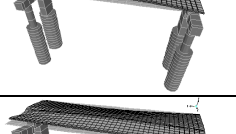
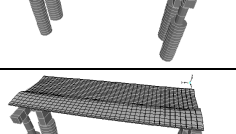
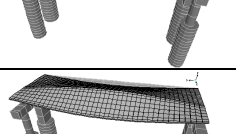
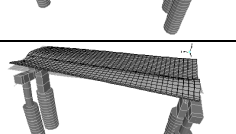
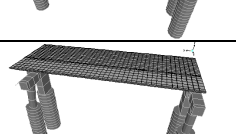
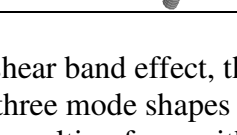
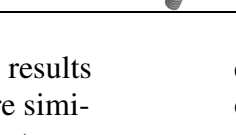
Table 2 shows the first six mode shapes and their corresponding frequencies for the Houfeng Bridge. It can be seen from Table 2 that, when there is no shear band effect, the first mode shape is the simultaneous to-and-fro vibration of girders and slabs along the x -direction (ignoring the friction force between the girder and the cap beam), with both corresponding frequencies close to zero. The second mode shape is the symmetrical up-and-down vibration of the horizontal centerline of the x -axis in the z -direction at a corresponding frequency of 2.875 Hz, with both ends of both the girder and the slab fixed. The third mode shape is the anti-symmetrical up-and-down vibration of the horizontal centerline of the x -axis in the z -direction, taking the

interface between the two joining slabs as the anti-symmetrical axis, at a corresponding frequency of 2.931 Hz with both ends of both the girder and the slab fixed. In the fourth mode, both ends of the x -axis of the girder and slab are fixed, with the interface of the parallel slabs vibrating up and down symmetrically about the x -axis along the z -direction. The other two parallel sides of the slabs vibrate up and down simultaneously in opposite directions about the x -axis in the z -direction, similar to the flapping of butterfly wings, with the corresponding frequency being 3.877 Hz. In the fifth mode, the entire structures of the adjacent bridges respectively rotate simultaneously and symmetrically in the y -direction about a line joining the x -axes of the bottom ends of the foundation. The corresponding frequency of this mode is 4.098 Hz. In the sixth mode,

the entire structures of the adjacent bridges respectively rotate simultaneously and anti-symmetrically in the y -direction about a line joining the x -axes

of the bottoms ends of the foundation. The corresponding frequency of mode six is 5.459 Hz.

Table 2. Influences of shear band on each mode shape and its corresponding frequency.

Mode No.	Mode Shape		Frequency(Hz)	
	Without shear band effect	With Shear band effect	Without shear band effect	With Shear band effect
1			≈ 0 (for frictionless interface between girders and cap beams)	≈ 0 (for frictionless interface between girders and cap beams)
2			2.875	2.460
3			2.931	2.496
4			3.877	3.081
5			4.098	3.318
6			5.459	3.782

With shear band effect, the results of the first three mode shapes are similar to those resulting from without shear band effect, with the frequencies of the second and third mode shapes being 2.460 Hz and 2.496 Hz, respectively. The results of the fourth mode shape is similar to that resulting from the fifth mode without the shear band

effects, with a corresponding frequency of 3.081Hz. The fifth mode shape has a partially large rotating magnitude of columns within the area with shear band effects, with a corresponding frequency of 3.318 Hz. The sixth mode shape is a combination of the cap beams of smaller volumes, and the piers and caisson foundations in the

area of partial shear band effects, rotating around the y -axis through the bottom ends of the caissons. The corresponding frequency is 3.782 Hz.

For the same bridge, from the results of the above study, it is found that shear band effects tend to soften the entire structure of the bridge, thereby lowering the corresponding frequencies of the respective modes. In the case study of the Houfeng Bridge, with or without shear band effects, the first three mode shapes are quite similar, with only the corresponding frequencies lowering by 14.4% and 14.8% for the second and third modes, respectively. After the fourth mode, not only are the mode shapes being influenced by shear band effects, the corresponding frequencies are more significantly affected, with decreases of 20.5%, 19.0%, and 30.7% in the corresponding frequencies, respectively, of the fourth, fifth, and sixth mode shapes.

As shown in Figure 5, the axial deflection of the Houfeng Bridge is equivalent to the first mode shape. Since friction forces are present between the girder and the cap beams, the corresponding frequency of the first mode shape slightly increased because of the presence of this friction force, thereby lowering the vibration magnitude of the first mode shape so that the Houfeng Bridge remained standing in the 1999 Jiji earthquake.

For the combination of the caisson, pier, and cap beams of the Houfeng Bridge, which were found lying on the riverbed after Typhoon Sinlaku as shown in Figure 10, since this type of damage is equivalent to given by the sixth mode shape, the collapse of the

Houfeng Bridge indeed resulted from shear band effects.

Result of the seismic response analysis

The finite element analysis program SAP 2000 V.14 was employed to perform a nonlinear seismic response analysis of the Houfeng Bridge. The Hilber–Hughes–Taylor- α method was selected for time integration, with a stiffness integration factor of 1.5, a damping integration factor of 1.0, a mass integration factor of 1.0, and a relative force convergence tolerance of 0.0001.

From Figure 26, it is found that in the selected seismic accelerogram, the maximum value in the x -direction is 0.369 g, occurring at 26.420 s, the maximum value in the y -direction is 0.512 g, occurring at 26.355 s, and the maximum value in the z -direction is 0.530 g, which occurred at 25.449 s of the elapsed time.

For the top of the piers at the severely grooved riverbed under shear band effects, the seismic displacement, velocity, and acceleration and corresponding accelerogram in the x -direction are as shown in Figures 27 through 29. Figure 27 shows a maximum seismic displacement of 0.379 cm under no shear band effects, occurring at 52.485 s, and a maximum seismic displacement of 1.326 cm under shear band effects, occurring at 52.995 s. Figure 28 shows a maximum seismic velocity of 9.530 cm/s for the top of the piers at the severely grooved riverbed under shear band effects, and a maximum seismic velocity of 31.337 cm/s, occurring at 53.205 s. Figure 29 shows a maximum seismic acceleration

of 0.520 g under no shear band effects, occurring at 53.075 s, and a maximum

seismic acceleration of 0.972 g, occurring at 79.475 s of the elapsed time.

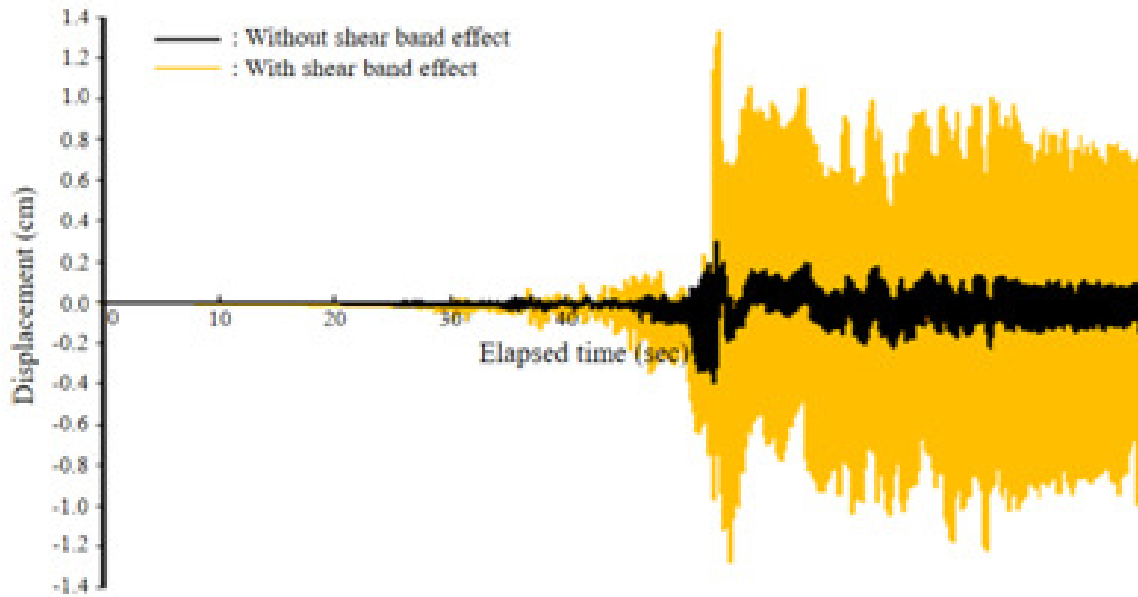


Figure 27. Influence of shear band effects on the x -direction seismic displacement response curve at the top of Pier 2.

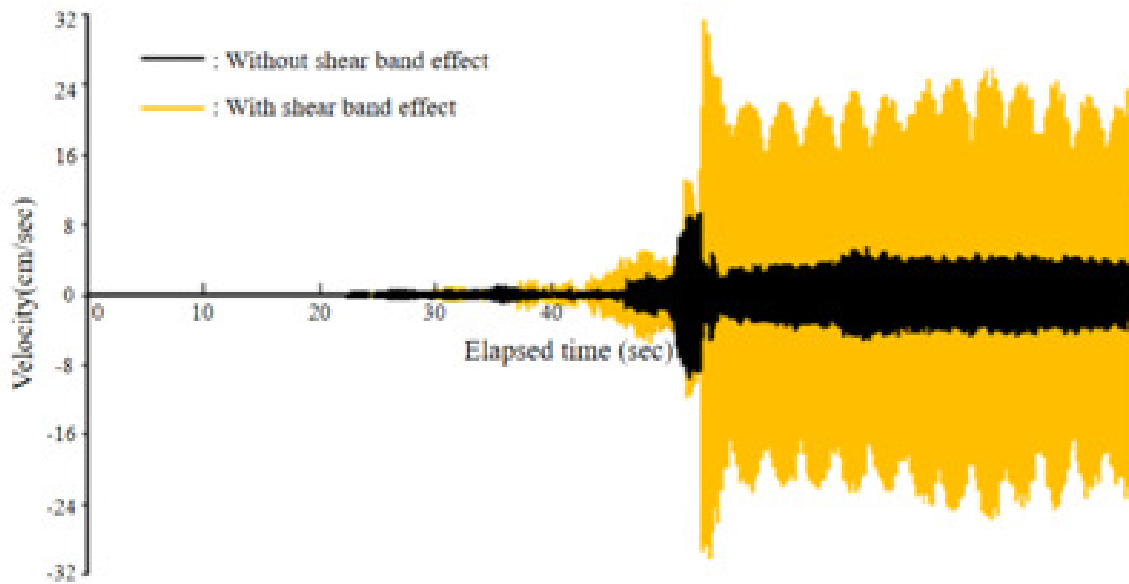


Figure 28. Influence of shear band effects on the x -direction seismic velocity response curve at the top of Pier 2.

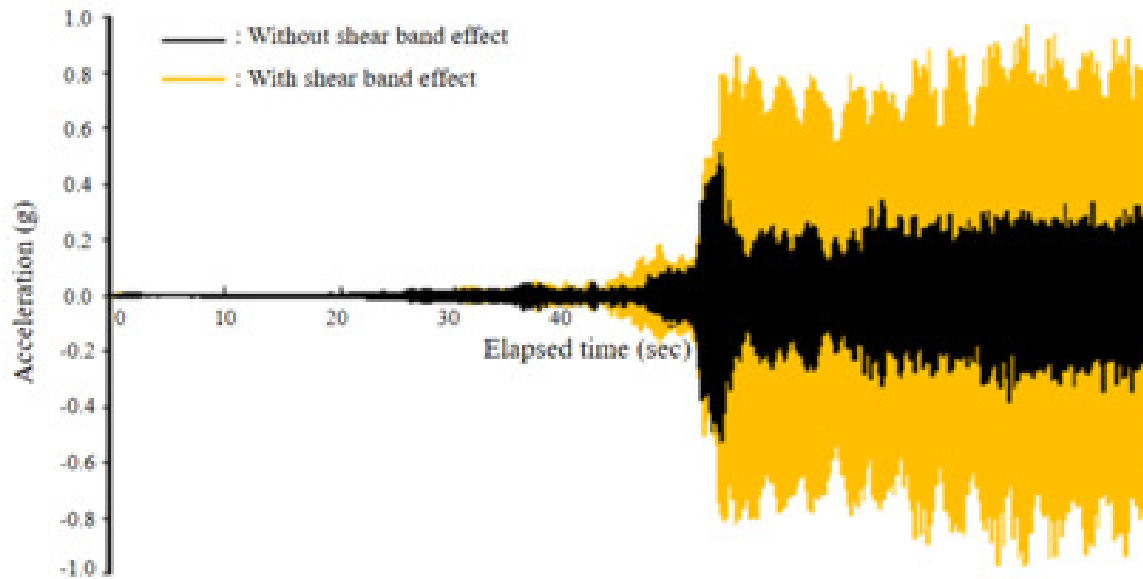


Figure 29. Influence of shear band effects on the x -direction seismic accelerogram at the top of Pier 2.

By comparing analysis results with and without shear band effects, it is found that the stiffness of the entire bridge significantly decreased under shear band effects. This resulted in a 250% increase of the maximum displacement at the top of Pier 2 in the x -direction, from 0.379 cm to 1.326 cm, a 229% increase of the maximum velocity, from 9.530 cm/s to 31.337 cm/s, and a 87% increase in maximum acceleration, from 0.520 g to 0.972 g. The maximum displacement time of occurrence increased from 52.485 s to 52.995 s, the maximum velocity from 51.925 s to 53.205 s, and the maximum acceleration from 53.075 s to 79.475 s.

Procedure for Fortification of Shear Banding When a Bridge Crosses a High Shear Strength Rock Riverbed

At present, the cause of bridge collapse in floods is considered to be riverbed scouring, so the bridge design code only requires fortification against riverbed scouring. However, riverbed scouring is only applicable to low shear strength soil riverbeds. For high shear strength rock riverbeds, after synthesizing the research results of this study, the following procedure is proposed to prevent bridge collapse during its design life:

- 1) Identify the location of the shear band and the rate of shear banding in the rock riverbed.
- 2) Calculate the maximum amount of shear banding that may exist in the design life of the bridge by using the rate of shear banding.
- 3) In the planning and design stage, the bridge's foundation is kept away

from the brittle-fractured shear-band rock riverbed.

- 4) The selection of the bridge type is based on the maximum amount of shear banding, and special considerations are made for the design of abutments, cap beams, and expansion joints.
- 5) After completion, continuous monitoring of the cumulative amount of shear banding should be carried out in order to adjust the abutment, cap beam, and expansion joints when the cumulative amount of shear banding reaches a pre-warning threshold value, so that the bridge can be protected from the influence of shear band effects during its design life.

Conclusions and Recommendations

Broadly, riverbeds can be divided into low shear strength soil riverbeds and high shear strength rock riverbeds, with collapses of bridges crossing low shear strength soil riverbeds and high shear strength rock riverbeds having different root causes. However, current bridge design specifications focus only on fortification against low shear strength soil riverbed scouring. As a result, many bridges crossing high shear strength rock riverbeds in Taiwan have collapsed, and their actual service life have been significantly shortened to 9 to 35 years. In view of this, the following five conclusions are drawn:

- 1) The collapse mechanism of bridges across low shear strength soil riverbeds is scouring, and the collapse mechanism of bridges across high shear strength rock

- riverbeds is deep grooving in the brittle-fractured shear bands.
- 2) The collapse mechanism of bridges across high shear strength rock riverbeds proposed in this study can not only make up for the shortcomings of current bridge design specifications, but can be further used to examine the major cause behind a bridge's collapse.
 - 3) Since soil riverbeds have low shear strength and the bridge's foundation is embedded up to 12 m or deeper in these soils, the bridge can remain stable even if the riverbed scours are 8 m or more. In fact, since the rock riverbed has high shear strength and the bridge's foundation is embedded 2-4 m or deeper in these rocks, they can collapse easily with the deep grooving effect in the shear bands.
 - 4) The deep grooving effect in the shear band will reduce the overall bridge stiffness, causing the bridge to undergo larger displacements, velocities, and accelerations under the same ground vibrations. The rock riverbed that constrains the caisson foundations of a bridge will therefore be brittle-fractured under excessive compression, and the loss of the shear-band rock will reduce the bearing capacity of the caisson foundation of a bridge, thereby endangering bridge safety.

Based on the above four conclusions, this study makes the following two recommendations:

- 1) In the past, bridge engineers did not consider shear band effects when designing bridges. As a result, the caisson foundations of the bridge

are embedded in the shear bands, so the stability of the bridge cannot be ensured. In light of this, it is recommended to forcibly adopt a procedure of fortification of the shear band of the bridge to ensure the bridge meets the performance targets after completion.

- 2) Taiwanese engineers only follow the bridge design specifications when designing bridges, but the bridge design specifications do not include the shear band effect, so it is recommended to quickly incorporate the shear band effect into bridge design specifications.

References

- Bicyclist, "Offroad Mud Exploratory Road," Website:
<https://www.mobile01.com/topicdetail.php?f=312&t=423223&p=2>, 2007.
- Central Weather Bureau, "Collection of Seismic Activities," Website:
https://www.cwb.gov.tw/V7/earthquake/rtd_eq.htm, 2020.
- Chiu, Yong-Fang, Hsieh, Ming-Zhi, Lin, Ya-Wen, Huang, Jin-Guo, Luo, Guan-Xian, Chai, Min-Gyi, Chen, Jia-Long, Yuan, Yu-Mei, Wang, Shu-Yu, Guo, Ting-Ming, **Discussion on Bridge Damage Caused by Typhoon Morakot**, Institute of Transportation, MOTC, Website:
<http://morakotdatabase.nstm.gov.tw/download-88flood.www.gov.tw/MorakotPublications/%E6%9B%B8%E6%9C%AC%E9%A1%9E%E6%AA%94%>

E6%A1%88/%E8%8E%AB%E6%8B%89%E5%85%8B%E9%A2%B1%E9%A2%A8%E9%80%A0%E6%88%90%E4%B8%BB%E8%A6%81%E6%A9%8B%E6%A2%81%E6%90%8D%E5%A3%9E%E4%B9%8B%E7%8F%BE%E5%9C%B0%E8%AA%BF%E6%9F%A5%E5%8F%8A%E7%81%BD%E5%9B%A0%E5%88%86%E6%9E%90.pdf, 2012.

Department of Transport and Main Roads, State of Queensland, **Bridge Scour Manual**, Website: <http://creativecommons.org/licenses/by/3.0/au/>, 2013.

Google Earth, Website: <http://www.google.com.tw/intl/zh-TW/earth/>, 2020.

GPS LAB, Website: <http://gps.earth.sinica.edu.tw/>, 2007.

Hertzberg, Richard W, **Deformation and fracture mechanics of engineering materials**, John Wiley & Sons, New York, 1983.

Hsu, Tse-Shan, **Capturing Localizations in Geotechnical Failures**, Ph.D. Dissertation, Civil Engineering in the school of Advanced Studies of Illinois Institute of Technology, 1987.

Hsu, Tse-Shan, "The Major Cause of Earthquake Disasters: Shear Bandings," Chapter 3 in **Earthquakes Forecast, Prognosis and Earthquake Resistant Construc-**

tion, Edited by Valentina Svalova, pp. 31-48, 2018.

Hsu, Tse-Shan and Hsieh, Yi-Lang, "An investigation on the falling bridge mechanism of the Houfong Bridge," **Taiwan Highway Engineering**, Vol. 35 No.10, pp. 2-15, 2009.

Jeng, Jin-Sing, "Dangerous Houfong Bridge becomes a broken bridge," Photo by Liao, Ren-Jie, Website: <http://magazine.sina.com/bg/newtaiwan/652/20080918/225373127.html>, 2008.

Keaton, Jefery R., Mishra, Su K. and Clopper, Paul E., **Scour at Bridge Foundations on Rock**, NCHRP Report 717, Transportation Research Board, Washington, D. C., 2012.

Khan, Mohiuddin A., **Flood Scour for Bridges and Highways: Prevention and Control of Soil Erosion**, McGraw Hill Professional, 2015.

Lagasse, P. F., Zevenbergen, L. W., Schall, J. D., & Clopper, P. E., **Bridge Scour and Stream Instability Countermeasures (NHI 01-003)**, U.S. Department of Transportation, Federal Highway Administration. Website: <http://isddc.dot.gov/OLPFiles/FHWA/010592.pdf>, 2001.

Lian, Yang-Wang, "Hsinchu Zhongzheng Bridge's pier exposed and concrete-groundsill work se-

verely cracked,” Flytiger Culture Enterprise Co., Ltd., Website: http://www.flytiger.com.tw/news_01.html, 2013.

Richardson, E. V. and Davis, S. R., **Evaluating scour at bridges, fourth edition description (NHI-01-001)**, U.S. Department of Transportation, Federal Highway Administration, Website: http://www.fhwa.dot.gov/engineering/hydraulics/library_arc.cfm?pub_number=17&id=37, 2001.

SAP2000, V18, Integrated Software for Structure Analysis and Design, Website: <https://www.csiamerica.com/products/sap2000>.

Tchalenko, J. S., "The evolution of kink-bands and the development of compression textures in sheared clays", **Tectonophysics**, Volume 6, pp. 159-174, 1968.

Warren, Linda P., **Scour at Bridges: Stream Stability and Scour Assessment at Bridges in Massachusetts**, U.S. Geological Survey, 2011.